Surface plasma attosource beamlines at ELI-ALPS

Sudipta Mondal, Mojtaba Shirozhan, Naveed Ahmed, Maïmouna Bocoum, Frederik Boehle, Aline Vernier, Stefan Haessler, Rodrigo Lopez-Martens, François Sylla, Cédric Sire, et al.

Surface-Plasma Attosource Beamlines at ELI-ALPS

SUDIPTA MONDAL[1], MOJTABA SHIROZHAN[1], NAVEED AHMED[1], MAÏMONA BOCOUM[2], FREDERIK BOEHLE[2], ALINE VERNIER[2], STEFAN HAESSLER[2], RODRIGO LOPEZ-MARTENS[1,2], FRANÇOIS SYLLA[3], CEDRIC SIRE[3], FABIEN QUÉRÉ[4], KWINTEN NELISSEN[1], KATALIN VARJÚ[1,5], DIMITRIS CHARALAMBIDIS[1,6,7], AND SUBHENDU KAHALY[1,*]

[1] *ELI-ALPS, ELI-HU Non-Profit Ltd., Dugonics tér 13, Szeged 6720, Hungary*
[2] *Laboratoire d'Optique Appliquée, ENSTA ParisTech, CNRS, Ecole Polytechnique, Université Paris-Saclay, 828 bd des Maréchaux, 91762 Palaiseau cedex, France*
[3] *SourceLAB SAS, 86 rue de Paris, F-91400 Orsay, France*
[4] *LIDYL, CEA, CNRS, Université Paris-Saclay, CEA Saclay, 91 191 Gif-sur-Yvette, France*
[5] *University of Szeged, Dugonics tér 13, H-6720 Szeged, Hungary*
[6] *Foundation for research and Technology Hellas (FORTH-IESL) P.O. Box 1385, 711 10 Heraklion, Greece*
[7] *Department of Physics, University of Crete, 71103 Heraklion, Greece*
[*] *Corresponding author: subhendu.kahaly@eli-alps.hu*

Compiled January 30, 2018

ELI-ALPS, one of the three pillars of Extreme Light Infrastructure (ELI) project, will be in a unique position to offer dedicated experimental platforms for ultrashort time-resolved investigations of strongly excited dynamical systems. The state of the art surface-plasma attosource (SPA) beamlines at ELI-ALPS are being designed and developed to enable new directions in plasma based attoscience research. The SPA beamlines will be driven by ultrashort, high peak power, high repetition rate lasers based on latest technology and are aimed to operate in a previously inaccessible regime of surface high-order harmonics generation. This endeavour involves R&D challenges and careful considerations. Here we discuss the physics of plasma attosources and their characteristics under such extreme conditions and the beamline functionalities that would facilitate these objectives. Finally we delineate the initial research possibilities with these sophisticated instruments.

OCIS codes: *(320.0320) Ultrafast optics; (340.7480) X-rays, soft x-rays, extreme ultraviolet (EUV);(320.7160) Ultrafast technology.*

http://dx.doi.org/10.1364/ao.XX.XXXXXX

1. INTRODUCTION

The wide ranging applications of intense coherent attosecond (1 $as = 10^{-18}$ s) light pulses [1] motivate the scientific community to channel substantial efforts into the development of such sources [2–4]. Several methods of generation of such light pulses have been explored [5] involving high-order harmonic generation (HHG) through the interaction of high-intensity femtosecond (fs) laser pulses with gaseous media (gas-HHG or GHHG) [6–8], lowly ionized plasma plumes [9–11], semiconductor crystals [12, 13] and plasma mirrors [4, 14]. All these potential avenues possess complementary features and remarkable uniqueness that will be explored in the different beamlines at the ELI-ALPS facility [15, 16].

One crucial parameter that controls the electron dynamics and determines the interaction regime of the HHG processes is the dimensionless vector potential, $a_0 = eE_0/m\omega_0 c = 8.85 \times 10^{-10} \times (I_0[W/cm^2]\lambda[\mu m]^2)^{1/2}$ (e, m, ω_0, c are the electronic charge and mass, fundamental laser frequency and the speed of light respectively. I_0, E_0 and λ are the peak intensity, electric field and the central wavelength) of the driving laser. Materials start breaking down at $a_0 \gtrsim 7 \times 10^{-4}$ and plasma is the only medium that can utilize modern high power femtosecond lasers operating at ultrahigh intensities (reaching $a_0 \geq 1$). Such a pulse focused on a dense flat target, instantly ionizes the surface in its leading edge triggering a plasma mirror (PM) that subsequently interacts with rest of the pulse-energy. The specific nature of the interaction depends strongly upon the driving laser properties (pulse duration, pulse shape, pulse energy, polarization), the interaction geometry (angle of incidence, focusing

configuration) and plasma characteristics (target plasma density and shape). Under appropriate conditions such an interaction can lead to nonlinear specular reflection of light with generation of new frequencies through surface high harmonic generation (SHHG) process [17]. Although GHHG [3] is the most conventional technique for implementing an attosource at lower intensities, SHHG [4, 17] approach is essential since it: (i) provides unique access to surface plasma metrology [18–21] important for interdisciplinary applications in the fields of laboratory astrophysics [22, 23], high energy density physics [24], development of laser-based energetic particle [25–27] and THz [28–30] sources; (ii) offers additional controls [31] and complementary features [5, 15] and (iii) has the potential to provide intense attosecond pulses with high conversion efficiencies [32, 33].

Two surface-plasma attosource (SPA) beamlines based on SHHG are being developed at ELI-ALPS. These are dedicated to HHG from plasma mirrors driven by state of the art lasers in the few-cycle moderately relativistic domain and many-cycle strongly relativistic domain. The SPA beamlines would operate mainly based on SHHG in two distinct interaction regimes: the coherent wake emission (CWE) [17, 34, 35] and relativistic oscillating mirror (ROM) [14, 36–38].

CWE is predominant at relatively lower laser intensities of $I_0\lambda^2 \sim 10^{14} - 10^{18}\, Wcm^{-2}\mu m^2$. Interaction at such intensities pulls out electron bunches from the surface, accelerates them in the combined laser and plasma field and then brings them back into the over-dense plasma. Charge density waves are excited along the plasma density gradient due to the returning electron bunches and the plasma oscillations re-emit light in the form of sub-cycle pulses. The cut-off P_{CWE} in the harmonic spectrum for CWE depends on the peak plasma frequency, which is determined by the material of the solid target [17, 34]. The cut-off is given by $P_{CWE} = \sqrt{n_e^{max}/n_c}$, where n_e^{max} and n_c are the maximum electron density in the generating medium and plasma critical density respectively. Simulation results exhibits a monotonic increase of CWE harmonic strength with laser intensity and follow a scaling law $\sim I_0^{2.6}$ [17, 35].

ROM is preponderant at $I_0\lambda^2 \gtrsim 10^{18}\, Wcm^{-2}\mu m^2$ where the periodic electron motion becomes relativistic. This results in nonlinear oscillations of the PM surface, which induces temporally localized sub-cycle modulations in the reflected laser field. In frequency domain this manifest as phase locked harmonics in the reflected laser spectrum. ROM SHHG spectral intensity $I(\omega_n)$ in general show a power law behaviour ($\propto (\omega_n/\omega_0)^{-p}$, ω_n being n^{th} harmonic frequency) followed by an exponential decay (rollover) [4, 17]. Under special conditions the process relates to the spikes in relativistic Lorentz γ factor of an apparent reflection point [37] and, $I(\omega_n) \sim (\omega_n/\omega_0)^{-8/3}$ upto a cut-off order $P_{ROM} = \sqrt{8\alpha}\gamma_{max}^3$ followed by rollover [14, 39], where γ_{max} is the maximum γ, and α is the second derivative of the surface speed at that moment.

Here we present the different aspects of the development of attosources with the SPA beamlines: the physics, the design and the challenges involved in realizing such a source that bear a great potential for the generation of intense attosecond pulses in the soft x-ray regime.

2. SURFACE PLASMA SOURCES WITH SYLOS AND HF

Fig. 1 summarizes the parameters of the two lasers that will be utilized for driving laser plasma interaction in the SPA beamlines. Depending on the focusing conditions, the SHHG beamline with SYLOS laser (SHHG-SYLOS) can achieve intensities

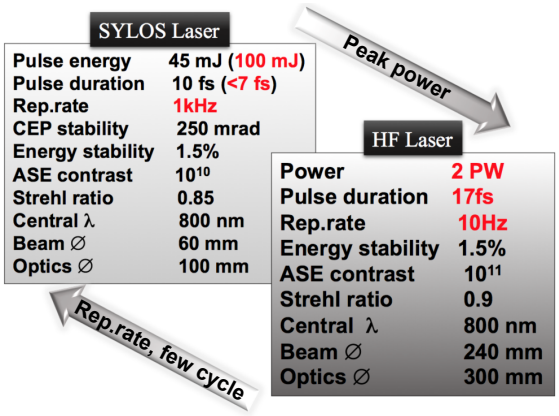

Fig. 1. Parameters of the SYLOS and HF primary sources that would drive complementary set of relativistic laser-plasma experiments in the SPA beamlines. The parameters in red are the values that would be achieved in the final phase.

$I_0 \sim 10^{18} - 10^{20}\, Wcm^{-2}$, while that with HF-PW (SHHG-HF) can reach intensities in the range $I_0 \sim 10^{21} - 10^{22}\, Wcm^{-2}$. With both these laser drivers, a dimensionless vector potential of $a_0 >> 1$ can thus be ensured, a condition essential for relativistic electron dynamics. This allows two complementary directions of research. The SYLOS (high power 1 kHz few cycle OPCPA laser with CEP stabilization [40]) based SHHG experiments would benefit from the few-cycle high-field driven CEP-controlled high-repetition-rate laser-plasma platform, giving access to sub-cycle control of electron dynamics and isolated attosecond pulse generation based on different mechanisms. The HF (2 PW laser system with 10 Hz repetition rate and pulse width 17 fs FWHM) driven beamline on the other hand would allow one to benefit from the intensity scaling of the SHHG spectral cut off and XUV flux and harness the strongly relativistic regime of interaction for the development of a PW-laser-driven 10-Hz attosource.

Relativistic laser interaction with PM is a complex process [41] and the two driver lasers operating under different conditions portray distinctive features in SHHG. The ultrafast evolution of plasma electron density and its effect on the reflected field can be qualitatively brought out in 1D3V Particle-in-Cell (PIC) simulations [4, 17, 42]. In such simulations oblique incidence can be dealt as normal incidence in a Lorentz boosted frame [43], making these virtual 2D. Below we perform 1D3V PIC simulations for SHHG under four typical cases with the following parameters:

- SHHG-SYLOS: The P- and S-polarized Gaussian laser pulse with normalized electric field amplitude a_0=6.9 and $\tau = 5$ fs (FWHM) duration interacts at an angle 45^o with a preformed overcritical singly ionized (z=1) Al plasma. The plasma exponential profile starts from $n_e = 0.2n_c$ with a gradient scale length $L = 0.1\lambda$ upto $n_e^{max} = 200n_c$. The spatial resolution (along x) of the simulation box is 1000 cells/λ and in each cell there are 2000 particles of both electrons and ions. The initial energies of electrons and mobile ions are 100 eV.

- SHHG-HF: The P- and S-polarized Gaussian laser pulse with normalized electric field amplitude a_0=69 and $\tau = 17$ fs (FWHM) duration interacts at an angle 45^o with a plasma of parameters same as for SYLOS.

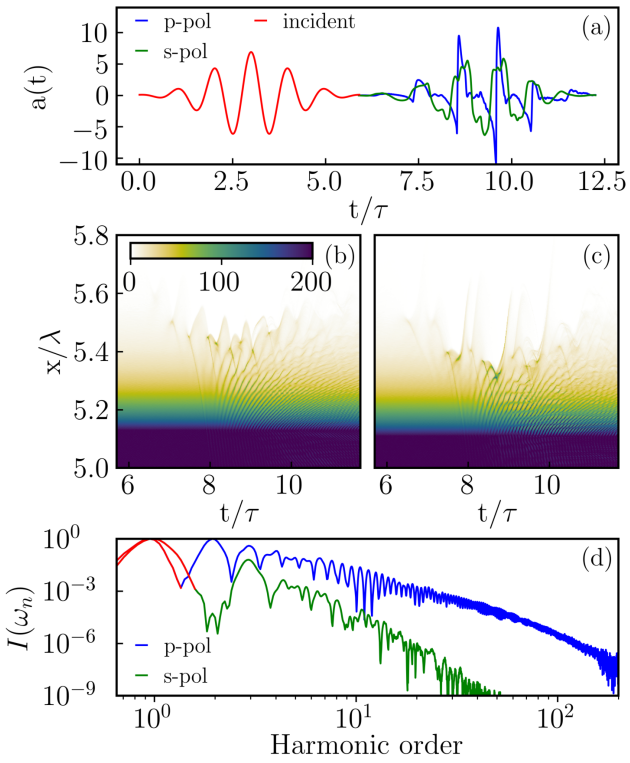

Fig. 2. PIC simulation results for SHHG-SYLOS. (a) incident and reflected pulses for both *S*- and *P*- polarized laser. (b) & (c) Spatio-temporal evolution of plasma electron density for *S*- & *P*- polarized incidence respectively, showing ultrafast density modulation that are responsible for SHHG. (d) $I(\omega_n)$ from simulations.

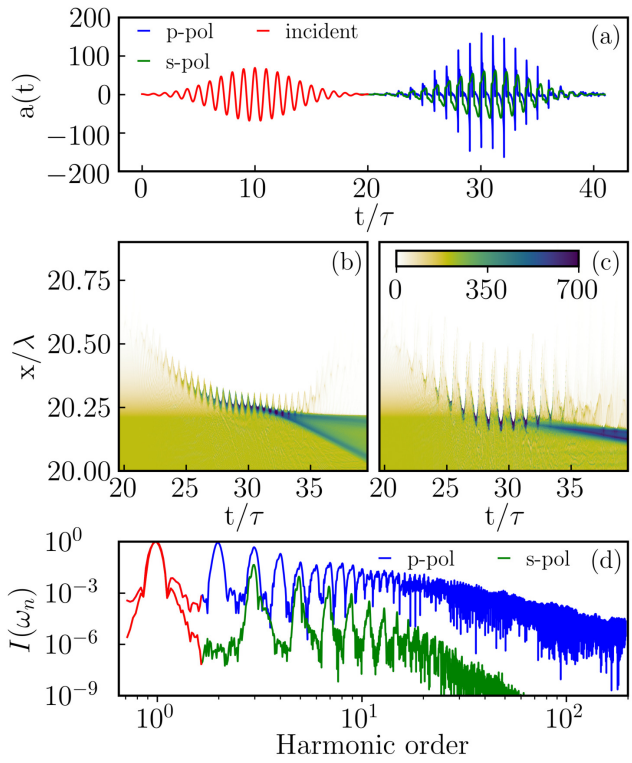

Fig. 3. PIC simulation results for SHHG-HF. (a) incident and reflected pulses for both *S*- and *P*- polarized irradiation. (b) & (c) Spatio-temporal evolution of the plasma electron density for *S*- & *P*- polarized cases respectively. Denting in the plasma density profile is observed. (d) $I(\omega_n)$ from simulations.

The incident and the reflected pulses under both *S*- and *P*-polarized irradiation from SYLOS and HF are shown in fig. 2-3 (a). The reflected pulses appear as harmonics in the frequency domain and are shown in fig. 2-3 (d). Harmonic spectra $I(\omega_n)$, normalized with respect to reflected $I(\omega_0)$ (red), for P-polarized (S-polarized) laser is shown in blue (green) line in fig. 2-3(d). Fig. 2 (b) & (c) show spatio-temporal behavior of $n_e(x,t)$ during laser plasma interaction at SHHG-SYLOS parameters, whereas fig. 3 (b) & (c) show the same for SHHG-HF. Summary observations and their implications are listed below:

(i) The ultra-fast plasma dynamics reveals two spikes per laser cycle for *S* compared to one for *P*-polarized case giving rise to odd HHG for *S* and odd-even HHG for *P* (fig. 2 (d)-3(d)).

(ii) Even τ =5 fs at such intensities contain multiple atto-pulses (evident also in the interference features in $I(\omega_n)$ in fig. 2(d)) as also observed in [44] implying additional considerations for generating isolated atto-pulses in SHHG-SYLOS.

(iii) For τ =17 fs, a longer interaction time allows denting (fig. 3(c)) on the plasma surface which might influence the divergence properties of the generated harmonic beam [18, 31]. Hence SHHG-HF design should take these considerations into account.

(iv) Due to higher focused intensity, SHHG-HF beamline will generate higher XUV flux for both P- & S- polarization which is evident from the normalized $I(\omega_n)$ shown in fig. 2-3(d). A higher XUV cut-off in SHHG-HF is also expected affecting the choice of XUV optics.

The estimated XUV pulse parameters which will be obtained in both the beamlines are summarized in table 1.

3. CHALLENGES IN BUILDING SUCH A SOURCE

SHHG in the regimes of operation of SPA beamlines, driven by the unique parameters of SYLOS and HF (fig. 1), has not been attempted before. The required developments and technical challenges of these beamlines are discussed below.

A. Tight focusing geometry

Since SHHG efficiency and cut-off frequency scales up with the driver laser intensity, it is imperative to drive the PM at the highest possible intensity at the focal point of the laser. This necessitates the use of low $f/\#$ focusing optics and hence strict aberration control, with wave front sensors and adaptive optics (fig. 6) to enhance spatial contrast in the interaction plane. For tightly focused fs pulses it is essential to pay attention to spatio temporal couplings (STC) [45] where the space and time variations of the laser field are coupled. STC is more often inherently present in this configuration [46–48] and can also be controlled to generate isolated atto pulses [49]. This entails both diagnosis and control of STC in the laser for optimal laser plasma interaction. Additionally for a given laser power tighter focusing puts more stringent requirements on pulse temporal contrast and is discussed next.

Surface Plasma Attosources	*SHHG-SYLOS*		*SHHG-HF*	
Attosecond pulse specs	ATP	SAP	Minimum achievable value	Realistic achievable value
Spectral range	8-60 eV	6-40 eV	100-200 eV	200-400 eV
XUV pulse energy at the source chamber	3-30 μJ	1-10 μJ	0.7 mJ ($10 < n < 20$)	7 mJ ($10 < n < 20$)
Pulse energy at the interaction chamber	1-10 μJ	0.3-3 μJ	data not available	
Pulse duration at the interaction chamber	< 5 fs	< 1 fs	< 10 fs (ATP) & < 500 as (SAP)	< 200 as (SAP)
Focal spot size at the interaction chamber	< 10 μm		$1 - 3$ μm	
XUV beam divergence	< 1 rad		$20 - 46$ mrad	
Polarization state	linear, horizontal		linear, horizontal	

Table 1. Expected initial parameters of the SHHG-SYLOS and SHHG-HF development beamlines (ATP: Attosecond pulse train and SAP: Single attosecond pulse configurations). The conservative estimation stems from the dearth of data under ELI-ALPS like interaction conditions.

B. Sub-λ plasma gradient control

High peak-power lasers often come with prepulses and pedestals at different levels and time scales. These produce a preplasma before the main pulse can interact. The preplasma expands slowly (in comparison to the incident laser pulse width) due to hydrodynamic pressure. An important parameter that determines the plasma expansion profile is the gradient scale length, $L = |n_e/(\nabla n_e)|$. Effective conversion of the driver laser to XUV attosecond pulses requires optimum preplasma scale-length ($L \simeq \lambda/50 - \lambda/10$ for CWE [17, 27] and $\simeq \lambda/10 - \lambda/5$ for ROM [50, 51]). Furthermore, the advantages of plasma shaping (section 5) can only be utilized while there is a sharp plasma-vacuum boundary at the beginning. This necessitates a high temporal contrast (depending on peak intensity) driver along with additional tools for fine control of L. The required temporal contrast for the fundamental laser pulse in the SHHG-SYLOS and SHHG-HF is 10^8 - 10^{10} and 10^{11} - 10^{12} respectively. Additional temporal cleaning could be essential for controlled interaction on top of the contrast that is achievable with the lasers directly.

C. High-repetition rate in focal plane targetry

SHHG-SYLOS operates at 1 kHz whereas SHHG-HF operates at 10 Hz (fig1). Both thus operate at the highest repetition rate compared to their class of SHHG sources. Hence, large targets are required for longer operation. For the case of SHHG-SYLOS large circular targets of a diameter 400 mm is designed for a net operation time of $\sim$ 1 h. The requirement of identical and reproducible interaction conditions at each laser shot, continuous operation, plasma gradient control combined with short Rayleigh length of laser focusing optics puts stringent constraints on target size, alignment and movement. Hence, high precision interferometric monitoring system with feedback control needs to be implemented for continuous supervision and operation of the target.

D. Optics and diagnostic protection issues

High repetition rate operation of the beamline produces a larger quantity of ablated materials and can degrade the expensive optics inside the vacuum chamber. This makes debris management issues a critical and integral part of such instruments. Adequate protection need to be designed for the reflective (flat mirrors), transmissive (XUV filters), focusing (off axis parabolic mirrors) and diffractive (flat-field gratings) optics to shield them from run-time debris. Diagnostics like micro channel plates (MCP), which would be placed in vacuum must also be shielded from the very bright incoherent background emission from plasma.

E. Radiation protection issues

High intensity laser solid interaction generates several types of ionizing radiations such as hard x-rays, and fast electrons and protons. Suitable protection against these radiations is thus required [52].

The vibration isolated multipurpose experimental bay, called building A, of ELI-ALPS consists of different isolated structural and operational units housing the lasers and the secondary source beamlines. This vibration isolated zone houses the primary lasers (laser area LA), the secondary sources (the beamlines) and the control rooms. Beam-transport delivers the lasers into the respective dedicated areas. The different beamlines are distributed into different dedicated lab spaces according to radiation shielding requirements. The dose and nature of those radiations depend on the laser intensity and require different levels of radiation shielding. Hence both the SPA beamlines would be operated from control room remotely during the experiment. One of the SPA beamlines, SHHG-SYLOS, will be driven by the SYLOS laser and is situated within the Medium Shielded Area (MTA), whereas the one driven by the HF PW laser, called SHHG-HF, is housed in the High Shielded Area (HTA). Radiation shielding is also planned locally in each beamline depending on specific types of directional and isotropic charge particle and radiation sources and is in the process of development.

For the optimal operability of the beamline and considering the activation issues the main interaction chambers are made from low Z material like Al.

F. EMP mitigation issues

High intensity femto-second laser pulses are shown to be capable of generating strong electro-magnetic pulses (EMP) both from gas jet [54] and solid surface [23, 53, 55] targets. In solids the EMP can ensue either from the motion of streaming charged particles escaping [25, 56] an initially neutral PM or the neutralizing circulation currents flowing through the target(-holder) at a comparatively slower time scale [55]. The target charging and neutralization dynamics eventually lead to huge electrical spikes or EMP over drastically different time scales [53].

Measurements conducted at different laboratories (See Fig. 4) have demonstrated extreme high EMP levels under comparable

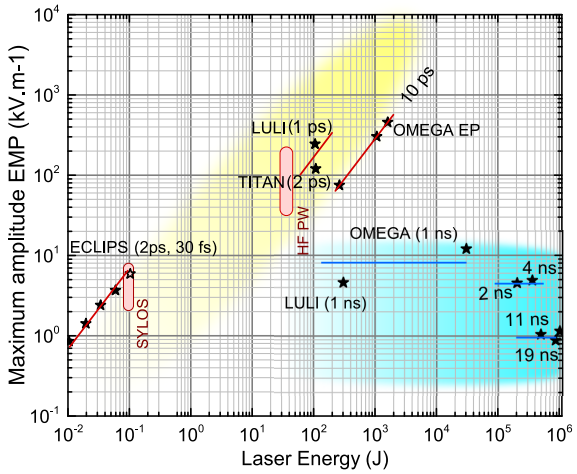

Fig. 4. Amplitude of the EMP electric field strength at 50 cm of the target from various laser facilities versus the laser energy. The data is taken from Ref. [53]. The red boxes show the expected electric field strength values for SHHG-SYLOS and SHHG-HF at ELI-ALPS. The red lines indicate linear scaling of the EMP-amplitude with the laser pulse energy given a certain pulse duration. The yellow shaded region corresponds to pico-femto second scale lasers while the cyan shaded region represents nano-second class.

intensities [53]. In the short pulse domain maximum amplitude of the EMP's is scaling linear with the laser pulse energy for a given pulse duration. This linear scaling is depicted by the red lines in Fig. 4. The red elliptical boxes in Fig. 4 indicate the expected electric field strengths of the drivers for the two SPA beamlines. At this moment it is unclear how this magnitude is scaling from pico-second towards femto-second pulse duration. However the projection on the 1 ps (for large pulse energy values) and the 30 fs equi-pulse-duration (for small pulse energy values) lines can be considered as a first order prediction for the laser systems present at ELI-ALPS.

Depending on the target and chamber geometry EMP-spectrum can extend from MHz toward the GHz regime and can induce excess noise in measurement and diagnostic devices. If strong enough, EMP might damage electronics outside and inside the target vacuum chamber, and even interfere with power and signal lines leading to perturbation and/or disruption of supply lines and signal communications. Therefore both the SPA beamlines need appropriate considerations specific to the design for EMP mitigation and protection. On the other hand, through investigation of laser generated EMP and its consequences is yet to be undertaken. Hence high repetition rate operation of the SPA beamlines would provide unique opportunity to pursue systematic measurements for comprehension of ultrashort laser generated EMP and its effects.

4. THE SURFACE PLASMA ATTOSOURCE BEAMLINES

A. The SYLOS 1 kHz SHHG beamline

SHHG-SYLOS capitalizes on the unique parameters of the driving laser SYLOS [40] and hence faces several technological challenges which have been discussed in section 3. In addition this beamline aims to cover both CWE and ROM regimes of SHHG by switching the focusing geometry to access different intensity domains.

A bird's eye view of SHHG-SYLOS is shown in fig. 5. An uncompressed SYLOS beam enters the beamline from the left in fig. 5. SHHG-SYLOS is divided into five separate sub-systems (**S1-S5**) for better management. Each sub-system is maintained under vacuum and are interconnected using vacuum connections and gate-valves. The details about each blocks is given below.

S1 is dedicated to the temporal cleaning at low intensity of the pulse by using a PM assembly. A single PM target will be installed on a high speed rotational stage. The incident pulse will interact with a continuously refreshed PM, which is synchronized with the SHHG target placed in **S4**. To provide long operation time, a large PM target with similar dimension of SHHG target will be installed. Near normal incidence of the laser pulse will increase the temporal contrast of the laser by two orders of magnitude without altering the polarization state. There is provision for variable on-target intensity for optimal compromise between tight shot spacing (more target usage), contrast cleaning and total transmission. **S1** allows high contrast (HC) mode of operation which can also be bypassed to utilize low contrast (LC) mode when necessary.

S2 is allotted for pulse compression and beam shaping. The uncompressed pulses will be compressed to $\leq$ 8 fs using a series of chirped mirrors. This sub-system also divides the beam into two separate beams, the main and an auxiliary beam (Aux-1), which can latter be used for plasma shaping. **S2** also houses a wedge pair assembly, which fine-tunes pulse compression in combination with the chirped mirror compressor. It can also be used to induce a wavefront-rotation at-focus during SHHG leading to generation of isolated attopulses through the attosecond lighthouse effect [49]. A deformable mirror assembly with a feedback loop from a wavefront diagnostic setup is installed here for online wavefront correction for Main beam. Any additional pulse shaping for both Main beam and Aux-1 may be housed in **S2**.

S3 houses spatio-temporal diagnostics of the compressed Main and Aux.1 beams before their interaction with the solid target installed in **S4**. **S3** also includes an assembly to recombine the 2 beams side-by-side before propagating into the interaction chamber **S4**. Translation mounted mirrors guide the attenuated beams to various characterization instruments either inside or outside the vacuum chamber. Diagnostics for temporal profiling of the Aux.1 and Main beam, temporal contrast measurement and characterization of spatio-temporal couplings in the Main beam are possible within **S3**.

S4 is the interaction/generation chamber where high intensity laser interacts with PM and high-order harmonics are generated. The design of this sub-system allows one to explore both CWE and ROM regimes in the same interaction chamber only by switching focusing geometry. The main laser beam will be focused on a polished target, which rotates at high speed to accommodate each laser spot on a fresh target with highest degree of stability to maintain same focusing condition. To attain conditions for ROM, relativistic intensity will be maintained by using off-axis parabolic mirror (OAP) with shorter focal length and HC mode of operation. CWE will be achieved by reducing intensity using longer focal length OAP at loose focusing geometry in combination with LC mode.

The Aux1 beam will be used to for plasma shaping. The details about the plasma shaping techniques which are planned to be implemented in the beamline are discussed in detail in section 5.

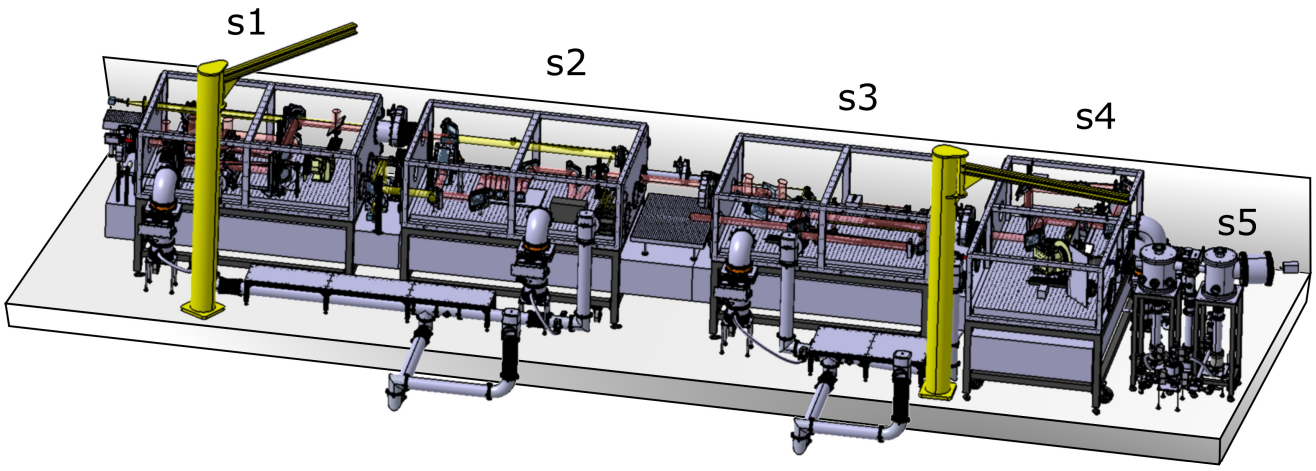

Fig. 5. Birds eye view of the 3d design of the complete SHHG-SYLOS beamline along with the different functional sub-systems **S1-S4**. The main driving laser propagates from left to right in the figure.

S5 is dedicated for XUV diagnostics and attosecond measurement. The XUV beam generated in **S4** will be transported to **S5** through a small hole placed at an intermediate beam focus. This will allow maintaining a pressure difference between the chambers by differential pumping. Attosecond characterization will be performed in this sub-system before any further application of the attosecond beam. This chamber can also be customized to accommodate specific attosecond measurement setups or to fulfill user demands for a particular experiment. The arrangement of the interaction chamber and endstation is shown in fig. 6.

B. The HF 10 Hz SHHG beamline

The SHHG-HF beamline comprises of 6 functional subsystems **H1-H6** and 3 turning boxes **T1-T3** which are housed in 7 high vacuum chambers (pressure of $\sim 10^{-6}$ mbar). Similar to the SHHG-SYLOS, this beamline is also capable of operating both in the CWE and ROM regime. All the subsystems are interconnected through appropriate vacuum components. A block diagram of the beamline is shown in the fig. 7. Individual sub-system and their role in the beamline is described below.

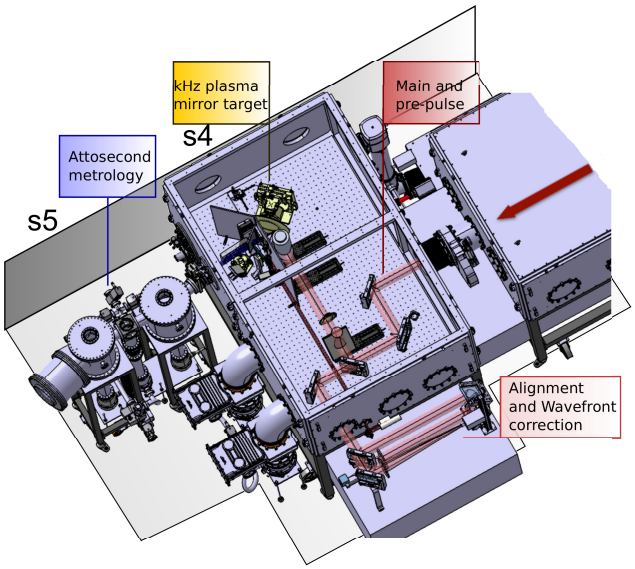

Fig. 6. SHHG SYLOS interaction chamber **S4** where the relativistic laser-plasma interaction takes place. The beam path and different constituent elements are demarcated. The red arrow indicates the direction of driving laser entry into **S4**. The working principle of **H5** is similar.

The uncompressed laser pulse enters the beamline through a turning box **T1** and is compressed in the grating based compressor **H1**. It then propagates back into **T1** which steers the pulse either to the PM chamber **H2** or a diagnostics chamber to characterize the compressed laser pulse. A diagnostic unit placed outside vacuum would have capabilities to measure the pulse duration, spatial contrast, beam spatial profile near-field and far-field, beam quality and various spatio-temporal couplings.

H2 is dedicated for PM cleaning that can further enhance the temporal contrast by $\sim 10^2$. The PM can be bypassed for a low contrast requirement and alignment purpose and the beam can be transported to the next subsystem.

H3 hosts the deformable mirror for active wavefront correction through a feedback loop from wavefront diagnostic setup situated further down the beamline. **H3** also serves as a turning box to steer the beam from **H2** into the attenuator **H6** in which the beam can be optionally attenuated (up to $10^{-8} - 10^{-9}$) for alignment purposes using several partially reflected dielectric mirrors. In operational mode, the attenuator system is bypassed and the beam passes through with full power.

T2 serves as a turning box which directs the attenuated/ unattenuated beam into the **H4** (laser shaping and metrology unit). A leak from **T2** is sent to a wavefront diagnostics setup for feedback on wavefront correction.

H4 houses various pulse diagnostics and components for shaping the amplitude, phase and polarization of the beam. These components can be selectively eliminated.An auxiliary beam (Aux) is generated at this stage which then goes through a delay line and follows the same path with the main beam.

T3 is used as a turning box to steer the beam into the interaction chamber **H5** and also holds the capability of creating prepulses if required for the interaction by using linearly translated mirrors to create 2 prepulses for inducing a plasma grating on the target. The mirrors can be removed from the beam path when no prepulses are required. This chamber can also be used to steer the beam for additional diagnostics offline.

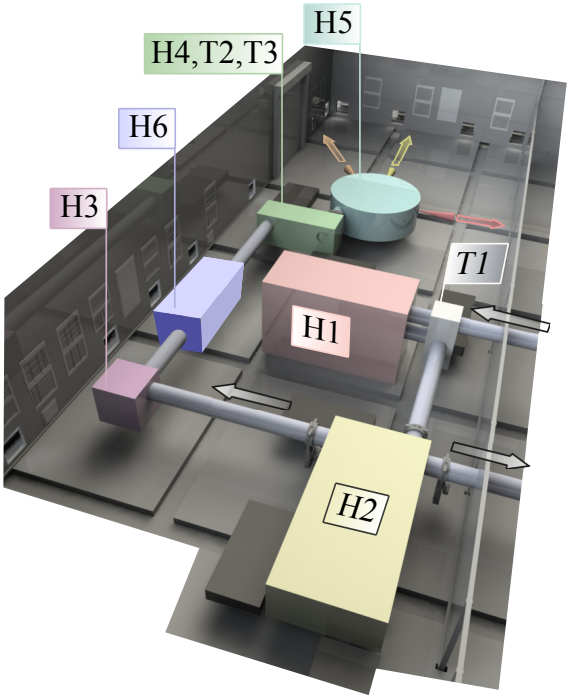

Fig. 7. Functional schematic of the 3d design of the complete SHHG HF beamline. The beam path and different constituent elements are demarcated. The gray arrow indicates the direction of driving laser.

H5 is the interaction chamber that holds the solid target for the generation of attosecond trains of XUV pulses. Two different types of interactions are potentially possible: transmissive interaction (gas/ultrathin target) and reflective interaction (solid target). OAPs with different focal lengths (500mm and 1300mm) will be used to obtain a loose/tight focusing on the solid target for CWE/ROM mechanisms of SHHG respectively. Depending on the kind of interaction (transmissive or reflective), the main beam as well as the attosecond pulse trains are delivered to different end stations. The interaction also generates particle beams normal to the target which can be guided to an end station for additional user experiments. A pair of XUV spectrometers that are collectively capable of measuring a harmonic spectral range between 80nm to 0.8nm can be used for characterization of the XUV pulse trains emerging from the target. Various other diagnostics are possible after the XUV pulses are shaped within this chamber.

The beamline also incorporates a portable alignment module which provides a visible beam with diameter of $\sim 20cm$ and a power of $\sim$ 30 mW and can be plugged into different subsystems for alignment purposes.

5. RESEARCH DIRECTIONS WITH SPA BEAMLINES

ELI-ALPS SPA platform provides enormous opportunity to develop the state of the art in SHHG technology further and use the unique laser parameters to surmount the challenges mentioned in sec. 3. The beamlines are designed (sec. 4) to pursue two different directions of investigations by: (i) permitting self-probing schemes for ultrafast laser-plasma experiments and (ii) utilizing SPA as a secondary source for specific user defined applications [1]. In addition it is possible to perform experiments on the primary lasers itself within different functional units.

In either case both SHHG-SYLOS and SHHG-HF need to be developed and calibrated before being ready for more challenging experiments. Utilization of the SPA beamlines require complete characterization of the generated secondary XUV beams which includes spatial, spectral as well as temporal measurements. The main different phases within the scope of this initial development work is illustrated in the fig. 8. Below we comment on two of the unique aspects of initial R&D with SPA.

A. Plasma shaping to control HHG

Originating from the steep surface plasma, HHG by this technique comes with important advantages. Along with the laser parameters, plasma shaping can be utilized to control the characteristics of the harmonic beam. By engineering the spatial phase of laser at focus and that of the light induced PM one can directly control the spatial features of the harmonic beam [31, 57]. Additionally longitudinal [50, 51] and transverse [18] plasma shaping can be utilized to control SHHG efficiency and XUV beam divergence.

A dedicated prepulse system is thus included in both the beamlines to control the PM surface. The gradient scale length L will be measured using spatial domain interferometry [58] where a transversly distributed pulse array is focused and used to generate diffraction pattern from an expanding preplasma. L is decoded from intensity modulations in far-field of the diffracted beam. Longitudinal plasma shaping allows optimizing SPA for specific laser parameters.

In addition, the prepulse system will also be used to create optically controlled transient plasma gratings which would interact with the main pulse for harmonic generation and XUV diffraction [18]. This transverse plasma shaping in combination with relativistic sub-cycle electron dynamics and ptychographic reconstruction techniques [19–21] provide a test bed for interdisciplinary research using spectrally resolved XUV spatial phase and amplitude metrology on strongly driven systems. These self-probing schemes of accessing knowledge on the relativistic plasma are possible to carry out in both the beamlines even without the CEP tagging.

B. Attosecond metrology

Apart from plasma based studies one major aim of SPA platform is to facilitate experiments with intense attopulses. This mandates implementing robust temporal metrology schemes and achieving tight focusing of the generated attopulses. Many of these techniques have already been developed for the GHHG scenario. However SHHG and GHHG have distinctive properties [5, 15] and thus a direct replication of existing attosecond measurement techniques is not always possible. These needs to be suitably adapted, developed and implemented for SPA beamlines. This provides additional scope for R&D in attosecond metrology of SPA. One needs to consider:

- The high divergence of SHHG-based sources poses a serious constraint for XUV beam transport and proper refocusing [59] which is prerequisite for application. The large bandwidth of attosecond pulses makes them very sensitive to aberrations causing spatio-temporal distortions in-focus which is detrimental to the attosecond properties of the pulse. Further, the grazing incidence optics used for reflecting high bandwidth XUV pulses easily add strong aberrations when not aligned perfectly. This needs special effort for optimal attosecond-beam-transport and refocusing.

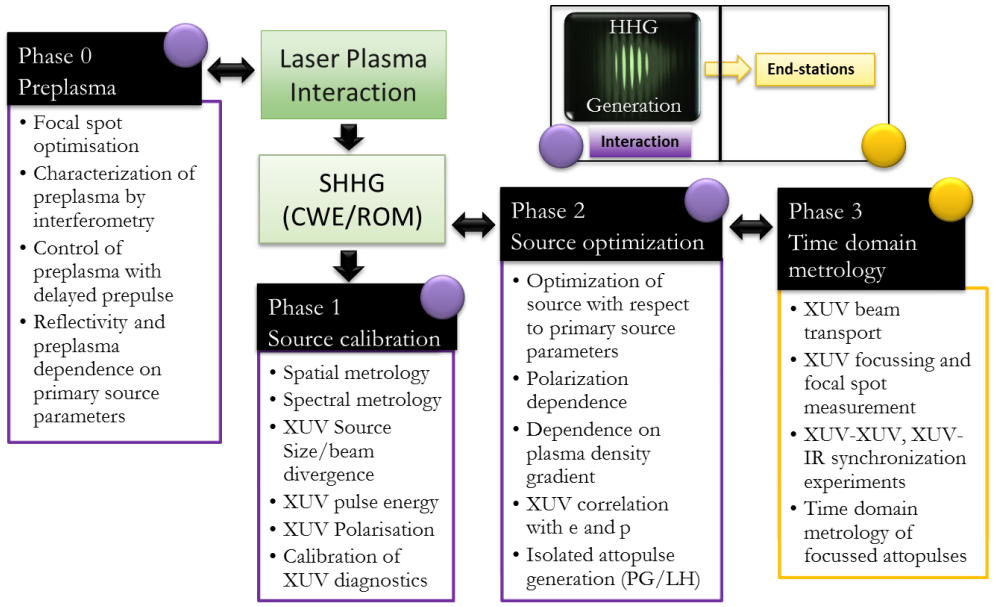

Fig. 8. Essential phases of research and development activity with SPA beamlines preceding more mature user based application experiments utilizing SHHG. The violet and orange solid circles correlates the source studies (list boxes) with the location within the beamlines (top left schematic).

- SPA driven by high intensity lasers are often limited by the number of attosecond bursts they can produce due to the requirement of fresh target surface. Reproducibility of interaction conditions demands a minimum number of attosecond bursts to be used for characterization. Hence development of single-shot measurement techniques would be preferable.

The existing XUV auto-correlation based techniques using two-photon induced ionization in gases [60, 61] can be extended to two-photon double ionization scenarios to accommodate required SHHG spectral window. Alternatively photoionization based approaches could be utilized. These approaches are restricted to photon energies above the ionization potentials of target gases (atomic to avoid all other "non-instantaneous" ionization channels and having negligible spin-orbit splitting to provide good spectral resolution). In this case the possibilities are either attosecond streaking (analyzed with FROG-CRAB [62] or ptychographic reconstruction [63]) or the perturbative PROOF [64] method for isolated attosecond pulses.

The above mentioned metrology schemes require a high resolution electron time-of-flight spectrometer and a long delay scan with attosecond temporal resolution. The development phase would permit probing the feasibility of single-shot autocorrelation of XUV pulses [65] using an ion microscope [66] as well as the suitability of single-shot streaking techniques [67, 68].

Ideally, most applications would require single attosecond pulses. On PM using laser pulses with duration more than two cycles this is difficult to achieve directly [44]. This means either implementation of one of the several methods (polarization gating [69, 70], lighthouse effect [71]) to isolate a single attosecond pulse from a train of SPA pulses (fig. 8) or take advantage of the conditions relativistic interaction with the PM [72]. Both these approaches would suitably be employed for SHHG-SYLOS and SHHG-HF.

6. CONCLUSIONS

The SPA beamlines at ELI-ALPS provide unique opportunities on plasma based attoscience research. These are driven by high repetition rate state of the art lasers and are at the cutting edge of technology and design engineering needing significant R&D before they are user ready as a routine secondary source. But they offer the possibility of the most intense laser based attosource and also among others, a unique route to interface laser plasma community with the attosecond science community.

7. ACKNOWLEDGMENTS

ELI-ALPS is supported by the European Union and co-financed by the European Regional Development Fund (GINOP-2.3.6-15-2015-00001).

REFERENCES

1. M. Reduzzi, P. Carpeggiani, S. Kühn, F. Calegari, M. Nisoli, S. Stagira, C. Vozzi, P. Dombi, S. Kahaly, P. Tzallas, D. Charalambidis, K. Varju, K. Osvay, and G. Sansone, "Advances in high-order harmonic generation sources for time-resolved investigations," J. Electron Spectros. Relat. Phenomena **204**, 257–268 (2015).
2. C. Winterfeldt, C. Spielmann, and G. Gerber, "Colloquium : Optimal control of high-harmonic generation," Reviews of Modern Physics **80**, 117–140 (2008).
3. F. Krausz and M. Ivanov, "Attosecond physics," Reviews of Modern Physics **81**, 163–234 (2009).
4. U. Teubner and P. Gibbon, "High-order harmonics from laser-irradiated plasma surfaces," Reviews of Modern Physics **81**, 445–479 (2009).
5. S. Chatziathanasiou, S. Kahaly, E. Skantzakis, G. Sansone, R. Lopez-Martens, S. Haessler, K. Varju, G. Tsakiris, D. Charalambidis, and P. Tzallas, "Generation of Attosecond Light Pulses from Gas and Solid State Media," Photonics **4**, 26 (2017).
6. P. B. Corkum, "Plasma perspective on strong field multiphoton ionization," Physical Review Letters **71**, 1994–1997 (1993).
7. L. Plaja, R. Torres, and A. Zaïr, eds., *Attosecond Physics*, vol. 177 of *Springer Series in Optical Sciences* (Springer Berlin Heidelberg, Berlin, Heidelberg, 2013).

8. Z. Chang, *Fundamentals of Attosecond Optics* (CRC Press, 2011).
9. L. B. Elouga Bom, S. Haessler, O. Gobert, M. Perdrix, F. Lepetit, J. F. Hergott, B. Carré, T. Ozaki, and P. Salières, "Attosecond emission from chromium plasma," Optics express **19**, 3677–3685 (2011).
10. R. A. Ganeev, *High-order harmonic generation in laser plasma plumes* (World Scientific, 2013).
11. M. A. Fareed, N. Thiré, S. Mondal, B. E. Schmidt, F. Légaré, and T. Ozaki, "Efficient generation of sub-100 eV high-order harmonics from carbon molecules using infrared laser pulses," Applied Physics Letters **108**, 124104 (2016).
12. G. Vampa, T. J. Hammond, N. Thiré, B. E. Schmidt, F. Légaré, C. R. McDonald, T. Brabec, and P. B. Corkum, "Linking high harmonics from gases and solids," Nature **522**, 462–464 (2015).
13. S. Ghimire, A. D. DiChiara, E. Sistrunk, P. Agostini, L. F. DiMauro, and D. a. Reis, "Observation of high-order harmonic generation in a bulk crystal," Nature Physics **7**, 138–141 (2010).
14. B. Dromey, S. Kar, C. Bellei, D. C. Carroll, R. J. Clarke, J. S. Green, S. Kneip, K. Markey, S. R. Nagel, P. T. Simpson, L. Willingale, P. McKenna, D. Neely, Z. Najmudin, K. Krushelnick, P. a. Norreys, and M. Zepf, "Bright Multi-keV Harmonic Generation from Relativistically Oscillating Plasma Surfaces," Physical Review Letters **99**, 085001 (2007).
15. S. Kühn, M. Dumergue, S. Kahaly, S. Mondal, M. Füle, T. Csizmadia, B. Farkas, B. Major, Z. Várallyay, F. Calegari, M. Devetta, F. Frassetto, E. Mänsson, L. Poletto, S. Stagira, C. Vozzi, M. Nisoli, P. Rudawski, S. Maclot, F. Campi, H. Wikmark, C. L. Arnold, C. M. Heyl, P. Johnsson, A. L'Huillier, R. Lopez-Martens, S. Haessler, M. Bocoum, F. Boehle, A. Vernier, G. Iaquaniello, E. Skantzakis, N. Papadakis, C. Kalpouzos, P. Tzallas, F. Lépine, D. Charalambidis, K. Varjú, K. Osvay, and G. Sansone, "The ELI-ALPS facility: the next generation of attosecond sources," Journal of Physics B: Atomic, Molecular and Optical Physics **50**, 132002 (2017).
16. D. Charalambidis, V. Chikán, E. Cormier, P. Dombi, J. A. Fülöp, C. Janáky, S. Kahaly, M. Kalashnikov, C. Kamperidis, S. Kühn, F. Lepine, A. L'Huillier, R. Lopez-Martens, S. Mondal, K. Osvay, L. Óvári, P. Rudawski, G. Sansone, P. Tzallas, Z. Várallyay, and K. Varjú, "The Extreme Light Infrastructure—Attosecond Light Pulse Source (ELI-ALPS) Project," in "Progress in Ultrafast Intense Laser Science XIII, Springer Series in Chemical Physics," K. Yamanouch, ed. (Springer, Cham, 2017), pp. 181–218.
17. C. Thaury and F. Quéré, "High-order harmonic and attosecond pulse generation on plasma mirrors: basic mechanisms," Journal of Physics B: Atomic, Molecular and Optical Physics **43**, 213001 (2010).
18. S. Monchocé, S. Kahaly, A. Leblanc, L. Videau, P. Combis, F. Réau, D. Garzella, P. D'Oliveira, P. Martin, and F. Quéré, "Optically Controlled Solid-Density Transient Plasma Gratings," Physical Review Letters **112**, 145008 (2014).
19. A. Leblanc, S. Monchocé, C. Bourassin-Bouchet, S. Kahaly, and F. Quéré, "Ptychographic measurements of ultrahigh-intensity laser–plasma interactions," Nature Physics **12**, 301–305 (2016).
20. A. Leblanc, S. Monchocé, H. Vincenti, S. Kahaly, J.-L. Vay, and F. Quéré, "Spatial Properties of High-Order Harmonic Beams from Plasma Mirrors: A Ptychographic Study," Physical Review Letters **119**, 155001 (2017).
21. A. Leblanc and F. Quéré, "In situ ptychographic measurements of high-order harmonic sources from plasma mirrors: A theoretical and numerical study," Physics of Plasmas **25**, 013112 (2018).
22. B. A. Remington, "High energy density laboratory astrophysics," in "Plasma Physics and Controlled Fusion," , vol. 47 (IOP Publishing, 2005), vol. 47, pp. A191–A203.
23. S. Kahaly, S. Mondal, G. R. Kumar, S. Sengupta, A. Das, and P. K. Kaw, "Polarimetric detection of laser induced ultrashort magnetic pulses in overdense plasma," Physics of Plasmas **16**, 043114 (2009).
24. R. P. Drake, *High-energy-density physics : fundamentals, inertial fusion, and experimental astrophysics* (Springer, 2006).
25. M. Thévenet, A. Leblanc, S. Kahaly, H. Vincenti, A. Vernier, F. Quéré, and J. Faure, "Vacuum laser acceleration of relativistic electrons using plasma mirror injectors," Nat. Phys. **12**, 355–360 (2015).
26. M. Thévenet, H. Vincenti, and J. Faure, "On the physics of electron ejection from laser-irradiated overdense plasmas," Physics of Plasmas **23**, 063119 (2016).
27. M. Bocoum, M. Thévenet, F. Böhle, B. Beaurepaire, A. Vernier, A. Jullien, J. Faure, and R. Lopez-Martens, "Anticorrelated Emission of High Harmonics and Fast Electron Beams From Plasma Mirrors," Physical Review Letters **116**, 185001 (2016).
28. H. Hamster, A. Sullivan, S. Gordon, W. White, and R. W. Falcone, "Subpicosecond, electromagnetic pulses from intense laser-plasma interaction," Physical Review Letters **71**, 2725–2728 (1993).
29. G.-Q. Liao, Y.-T. Li, C. Li, S. Mondal, H. A. Hafez, M. A. Fareed, T. Ozaki, W.-M. Wang, Z.-M. Sheng, and J. Zhang, "Terahertz emission from two-plasmon-decay induced transient currents in laser-solid interactions," Physics of Plasmas **23**, 013104 (2016).
30. S. Mondal, H. A. Hafez, X. Ropagnol, and T. Ozaki, "MV/cm terahertz pulses from relativistic laser-plasma interaction characterized by nonlinear terahertz absorption bleaching in n-doped InGaAs," Optics Express **25**, 17511 (2017).
31. H. Vincenti, S. Monchocé, S. Kahaly, G. Bonnaud, P. Martin, and F. Quéré, "Optical properties of relativistic plasma mirrors," Nature communications **5** (2014).
32. G. D. Tsakiris, K. Eidmann, J. Meyer-ter Vehn, and F. Krausz, "Route to intense single attosecond pulses," New Journal of Physics **8**, 19–19 (2006).
33. P. Heissler, A. Barna, J. M. Mikhailova, G. Ma, K. Khrennikov, S. Karsch, L. Veisz, I. B. Földes, and G. D. Tsakiris, "Multi-μJ harmonic emission energy from laser-driven plasma," Applied Physics B **118**, 195–201 (2015).
34. F. Quéré, C. Thaury, P. Monot, S. Dobosz, P. Martin, J.-P. Geindre, and P. Audebert, "Coherent Wake Emission of High-Order Harmonics from Overdense Plasmas," Physical Review Letters **96**, 125004 (2006).
35. A. Malvache, A. Borot, F. Quéré, and R. Lopez-Martens, "Coherent wake emission spectroscopy as a probe of steep plasma density profiles," Phys. Rev. E **87**, 035101 (2013).
36. D. Von der Linde and K. Rzazewski, "High-order optical harmonic generation from solid surfaces," Applied Physics B: Lasers and Optics **63**, 499–506 (1996).
37. T. Baeva, S. Gordienko, and A. Pukhov, "Theory of high-order harmonic generation in relativistic laser interaction with overdense plasma," Physical Review E **74**, 046404 (2006).
38. S. V. Bulanov, T. Z. Esirkepov, M. Kando, and J. Koga, "Relativistic mirrors in laser plasmas (analytical methods)," Plasma Sources Science and Technology **25**, 053001 (2016).
39. B. Dromey, M. Zepf, A. Gopal, K. Lancaster, M. Wei, K. Krushelnick, M. Tatarakis, N. Vakakis, S. Moustaizis, R. Kodama *et al.*, "High harmonic generation in the relativistic limit," Nature physics **2**, 456 (2006).
40. R. Budriūnas, T. Stanislauskas, J. Adamonis, A. Aleknavičius, G. Veitas, D. Gadonas, S. Balickas, A. Michailovas, and A. Varanavičius, "53 W average power CEP-stabilized OPCPA system delivering 55 TW few cycle pulses at 1 kHz repetition rate," Optics Express **25**, 5797 (2017).
41. T. Kluge, C. Gutt, L. G. Huang, J. Metzkes, U. Schramm, M. Bussmann, and T. E. Cowan, "Using X-ray free-electron lasers for probing of complex interaction dynamics of ultra-intense lasers with solid matter," Phys. Plasmas **21**, 033110 (2014).
42. R. Lichters, J. Meyer-ter Vehn, and A. Pukhov, "Short-pulse laser harmonics from oscillating plasma surfaces driven at relativistic intensity," Physics of Plasmas **3**, 3425 (1996).
43. A. Bourdier, "Oblique incidence of a strong electromagnetic wave on a cold inhomogeneous electron plasma. Relativistic effects," Physics of Fluids **26**, 1804 (1983).
44. P. Heissler, R. Hörlein, J. M. Mikhailova, L. Waldecker, P. Tzallas, A. Buck, K. Schmid, C. M. S. Sears, F. Krausz, L. Veisz, M. Zepf, and G. D. Tsakiris, "Few-Cycle Driven Relativistically Oscillating Plasma Mirrors: A Source of Intense Isolated Attosecond Pulses," Physical Review Letters **108**, 235003 (2012).
45. S. Akturk, X. Gu, P. Bowlan, and R. Trebino, "Spatio-temporal couplings in ultrashort laser pulses," Journal of Optics **12**, 093001 (2010).
46. S. Kahaly, S. Monchocé, V. Gallet, O. Gobert, F. Réau, O. Tcherbakoff, P. D'Oliveira, P. Martin, and F. Quéré, "Investigation of amplitude spatio-temporal couplings at the focus of a 100 TW-25 fs laser," Applied Physics

Letters **104**, 054103 (2014).
47. V. Gallet, S. Kahaly, O. Gobert, and F. Quéré, "Dual spectral-band interferometry for spatio-temporal characterization of high-power femtosecond lasers." Optics letters **39**, 4687–90 (2014).
48. G. Pariente, V. Gallet, A. Borot, O. Gobert, and F. Quéré, "Space–time characterization of ultra-intense femtosecond laser beams," Nature Photonics **10**, 547–553 (2016).
49. J. A. Wheeler, A. Borot, S. Monchocé, H. Vincenti, A. Ricci, A. Malvache, R. Lopez-Martens, and F. Quéré, "Attosecond lighthouses from plasma mirrors," Nature Photonics **6**, 829–833 (2012).
50. F. Dollar, P. Cummings, V. Chvykov, L. Willingale, M. Vargas, V. Yanovsky, C. Zulick, A. Maksimchuk, A. G. R. Thomas, and K. Krushelnick, "Scaling High-Order Harmonic Generation from Laser-Solid Interactions to Ultrahigh Intensity," Physical Review Letters **110**, 175002 (2013).
51. S. Kahaly, S. Monchocé, H. Vincenti, T. Dzelzainis, B. Dromey, M. Zepf, P. Martin, and F. Quéré, "Direct Observation of Density-Gradient Effects in Harmonic Generation from Plasma Mirrors," Physical Review Letters **110**, 175001 (2013).
52. F. Borne, D. Delacroix, J. M. Gel, D. Mass, and F. Amiranoff, "Radiation Protection for an Ultra-high Intensity Laser," Radiation Protection Dosimetry **102**, 61–70 (2002).
53. A. Poyé, J.-L. Dubois, F. Lubrano-Lavaderci, E. D'Humières, M. Bardon, S. Hulin, M. Bailly-Grandvaux, J. Ribolzi, D. Raffestin, J. J. Santos, P. Nicolaï, and V. Tikhonchuk, "Dynamic model of target charging by short laser pulse interactions," Phys. Rev. E **92**, 043107 (2015).
54. A. Flacco, J. Vieira, A. Lifschitz, F. Sylla, S. Kahaly, M. Veltcheva, L. O. Silva, and V. Malka, "Persistence of magnetic field driven by relativistic electrons in a plasma," Nature Physics **11**, 409–413 (2015).
55. A. Poyé, S. Hulin, M. Bailly-Grandvaux, J. L. Dubois, J. Ribolzi, D. Raffestin, M. Bardon, F. Lubrano-Lavaderci, E. D'Humières, J. J. Santos, P. Nicolaï, and V. Tikhonchuk, "Physics of giant electromagnetic pulse generation in short-pulse laser experiments," Phys. Rev. E - Stat. Nonlinear, Soft Matter Phys. **91**, 043106 (2015).
56. M. J. Mead, D. Neely, J. Gauoin, R. Heathcote, and P. Patel, "Electromagnetic pulse generation within a petawatt laser target chamber," Review of Scientific Instruments **75**, 4225–4227 (2004).
57. F. Quéré, C. Thaury, J. P. Geindre, G. Bonnaud, P. Monot, and P. Martin, "Phase properties of laser high-order harmonics generated on plasma mirrors," Physical Review Letters **100**, 1–4 (2008).
58. M. Bocoum, F. Böhle, A. Vernier, A. Jullien, J. Faure, and R. Lopez-Martens, "Spatial-domain interferometer for measuring plasma mirror expansion," Optics Letters **40**, 3009–3012 (2015).
59. C. Bourassin-Bouchet, M. M. Mang, F. Delmotte, P. Chavel, and S. de Rossi, "How to focus an attosecond pulse," Optics Express **21**, 2506–2520 (2013).
60. Y. Nomura, R. Hörlein, P. Tzallas, B. Dromey, S. Rykovanov, Z. Major, J. Osterhoff, S. Karsch, L. Veisz, M. Zepf, D. Charalambidis, F. Krausz, and G. D. Tsakiris, "Attosecond phase locking of harmonics emitted from laser-produced plasmas," Nature Physics **5**, 124–128 (2009).
61. R. Hörlein, Y. Nomura, P. Tzallas, S. G. Rykovanov, B. Dromey, J. Osterhoff, Z. Major, S. Karsch, L. Veisz, M. Zepf, D. Charalambidis, F. Krausz, and G. D. Tsakiris, "Temporal characterization of attosecond pulses emitted from solid-density plasmas," New Journal of Physics **12**, 043020 (2010).
62. F. Quéré, Y. Mairesse, and J. Itatani, "Temporal characterization of attosecond XUV fields," Journal of Modern Optics **52**, 339–360 (2005).
63. M. Lucchini, M. H. Brügmann, A. Ludwig, L. Gallmann, U. Keller, and T. Feurer, "Ptychographic reconstruction of attosecond pulses," Optics Express **23**, 29502–29513 (2015).
64. M. Chini, S. Gilbertson, S. D. Khan, and Z. Chang, "Characterizing ultrabroadband attosecond lasers," Optics Express **18**, 13006 (2010).
65. G. Kolliopoulos, P. Tzallas, B. Bergues, P. A. Carpeggiani, P. Heissler, H. Schröder, L. Veisz, D. Charalambidis, and G. D. Tsakiris, "Single-shot autocorrelator for extreme-ultraviolet radiation," Journal of the Optical Society of America B **31**, 926 (2014).
66. N. Tsatrafyllis, B. Bergues, H. Schröder, L. Veisz, E. Skantzakis, D. Gray, B. Bodi, S. Kuhn, G. D. Tsakiris, D. Charalambidis *et al.*, "The ion microscope as a tool for quantitative measurements in the extreme ultraviolet," Scientific reports **6**, 21556 (2016).
67. U. Frühling, M. Wieland, M. Gensch, T. Gebert, B. Schütte, M. Krikunova, R. Kalms, F. Budzyn, O. Grimm, J. Rossbach, E. Plönjes, and M. Drescher, "Single-shot terahertz-field-driven X-ray streak camera," Nature Photonics **3**, 523–528 (2009).
68. W. Helml, A. R. Maier, W. Schweinberger, I. Grguraš, P. Radcliffe, G. Doumy, C. Roedig, J. Gagnon, M. Messerschmidt, S. Schorb, C. Bostedt, F. Grüner, L. F. DiMauro, D. Cubaynes, J. D. Bozek, T. Tschentscher, J. T. Costello, M. Meyer, R. Coffee, S. Düsterer, A. L. Cavalieri, and R. Kienberger, "Measuring the temporal structure of few-femtosecond free-electron laser X-ray pulses directly in the time domain," Nature Photonics **8**, 950–957 (2014).
69. S. G. Rykovanov, M. Geissler, J. Meyer-ter Vehn, and G. D. Tsakiris, "Intense single attosecond pulses from surface harmonics using the polarization gating technique," New Journal of Physics **10**, 025025 (2008).
70. M. Yeung, J. Bierbach, E. Eckner, S. Rykovanov, S. Kuschel, A. Sävert, M. Förster, C. Rödel, G. G. Paulus, S. Cousens, M. Coughlan, B. Dromey, and M. Zepf, "Noncollinear Polarization Gating of Attosecond Pulse Trains in the Relativistic Regime," Physical Review Letters **115**, 193903 (2015).
71. F. Quéré, H. Vincenti, A. Borot, S. Monchocé, T. J. Hammond, K. T. Kim, J. A. Wheeler, C. Zhang, T. Ruchon, T. Auguste, J. F. Hergott, D. M. Villeneuve, P. B. Corkum, and R. Lopez-Martens, "Applications of ultrafast wavefront rotation in highly nonlinear optics," Journal of Physics B: Atomic, Molecular and Optical Physics **47**, 124004 (2014).
72. Z.-Y. Chen and A. Pukhov, "Bright high-order harmonic generation with controllable polarization from a relativistic plasma mirror," Nature Communications **7**, 12515 (2016).